4 J. Aaron, K. Travis, N. Harrison and K. Sokolov, *Nano Lett.*, 2009, **9**, 3612.
5 Y. E. Korchev, C. L. Bashford, M. Milovanovic, I. Vodyanoy and M. J. Lab, *Biophys. J.*, 1997, **73**, 653.
6 A. I. Shevchuk, P. Hobson, M. J. Lab, D. Klenerman, N. Krauzewicz and Y. E. Korchev, *Pfluegers Arch.*, 2008, **456**, 227.
7 A. Schulte and W. Schuhmann, *Angew. Chem., Int. Ed.*, 2007, **46**, 8760.
8 A. J. Bard, X. H. Liu, M. M. Ramsey, X. L. Chen, D. Koley and M. Whiteley, *Proc. Natl. Acad. Sci. U. S. A.*, 2011, **108**, 2668.
9 Z. F. Ding, X. C. Zhao, S. Lam and J. Jass, *Electrochem. Commun.*, 2010, **12**, 773.
10 Y. Takahashi, T. Miyamoto, H. Shiku, R. Asano, T. Yasukawa, I. Kumagai and T. Matsue, *Anal. Chem.*, 2009, **81**, 2785.
11 Y. Xue, L. Ding, J. Lei, F. Yan and H. Ju, *Anal. Chem.*, 2010, **82**, 7112.
12 Y. Takahashi, H. Shiku, T. Murata, T. Yasukawa and T. Matsue, *Anal. Chem.*, 2009, **81**, 9674.
13 P. Sun, F. O. Laforge, T. P. Abeyweera, S. A. Rotenberg, J. Carpino and M. V. Mirkin, *Proc. Natl. Acad. Sci. U. S. A.*, 2008, **105**, 443.
14 D. J. Leszczyszyn, J. A. Jankowski, O. H. Viveros, E. J. Diliberto, J. A. Near and R. M. Wightman, *J. Biol. Chem.*, 1990, **265**, 14736.
15 A. L. Barker, J. V. Macpherson, C. J. Slevin and P. R. Unwin, *J. Phys. Chem. B*, 1998, **102**, 1586.
16 H. Yamada, T. Matsue and I. Uchida, *Biochem. Biophys. Res. Commun.*, 1991, **180**, 1330.
17 R. Asano, Y. Sone, K. Makabe, K. Tsumoto, H. Hayashi, Y. Katayose, M. Unno, T. Kudo and I. Kumagai, *Clin. Cancer Res.*, 2006, **12**, 4036.
18 M. Nishizawa, K. Takoh and T. Matsue, *Langmuir*, 2002, **18**, 3645.
19 H. Q. Luo, H. Shiku, A. Kumagai, Y. Takahashi, T. Yasukawa and T. Matsue, *Electrochem. Commun.*, 2007, **9**, 2703.
20 T. Murata, T. Yasukawa, H. Shiku and T. Matsue, *Biosens. Bioelectron.*, 2009, **25**, 913.

Sensors and Actuators B 160 (2011) 923–928

Contents lists available at SciVerse ScienceDirect

Sensors and Actuators B: Chemical

journal homepage: www.elsevier.com/locate/snb

Amperometric detection of DNA hybridization using a multi-point, addressable electrochemical device

Xi Zhu[a,b], Kosuke Ino[b], Zhenyu Lin[a], Hitoshi Shiku[b], Guonan Chen[a], Tomokazu Matsue[b,c,*]

[a] Ministry of Education Key Laboratory of Analysis and Detection for Food Safety, Fujian Provincial Key Laboratory of Analysis and Detection for Food Safety, Department of Chemistry, Fuzhou University, Fuzhou, Fujian 350002, China
[b] Graduate School of Environmental Studies, Tohoku University, 6-6-11-604 Aramaki-Aoba, Aoba, Sendai 980-8579, Japan
[c] Advanced Institute of Materials Research, Tohoku University, 2-1-1 Katahira, Aoba, Sendai 980-8579, Japan

ARTICLE INFO

Article history:
Received 6 July 2011
Received in revised form 29 August 2011
Accepted 3 September 2011
Available online 10 September 2011

Keywords:
DNA detection
Addressable
Electrochemical detection
Multipoint detection

ABSTRACT

A novel device was designed for the multipoint addressable detection of DNA hybridization. Row and column electrodes array were orthogonally arranged, and the microwells were assembled on the crossing points of the row/column electrodes to form a 4 × 4 microwell array. Amperometric signals at the individual microwells could be detected separately on the basis of redox cycling of localized electroactive species occurring between the electrodes. Immobilization and hybridization of DNA could block the redox cycling of $Fe(CN)_6^{4-}/Fe(CN)_6^{3-}$ at the designated microwells, resulting in the reduction of current response. This device had been used to detect DNA hybridization with excellent sensitivity (0.03 μM) and selectivity. The device can be applied to comprehensive and high-throughput detection and imaging of biochemical species.

1. Introduction

The detection of DNA hybridization is of central importance to the diagnosis and treatment of genetic diseases, for the detection of infectious agents, and for reliable forensic analysis. Hence, various DNA biosensors have been developed based on the immobilization of a single-stranded DNA (ssDNA) probe onto a surface to recognize its complementary DNA target sequence by hybridization. Contrary to DNA biosensors that allow single-shot measurements, DNA arrays allow simultaneous detection and analysis of patterns of expression of thousands of genes in a single experiment [1–4]. Hence, the development of DNA arrays would be more desirable. Because fluorescence measurement usually has a high sensitivity and a variety of tools for performing the measurements are commercially available, many DNA arrays based on fluorescence detection are developed [5–10]. Although DNA arrays based on fluorescence detection are a powerful tool that provides complex and informative data from nucleic acid sequences, they need fluorescence scanners that are inherently costly and not transportable [11], which limited the widespread use of DNA fluorescence arrays for point-of-care testing or as a routine diagnostics tool. Another alternative form of detection utilized in DNA array is electrochemical detection, which possesses the advantages of high sensitivity, small size, low cost, and compatibility with micromanufacturing technology [12,13]. So far, various DNA arrays based on electrochemical detection have been developed [14–21]. All above arrays were performed by connecting each electrode to a corresponding bond pad in the 1:1 mode. However, the number of individually addressable electrodes is limited, due to sufficient space for bond pads is not available on the chip border.

Recently, a novel multipoint addressable electrochemical device has been reported [22,23]. This device consists of orthogonally arranged arrays of rows and columns of electrodes. Based on the local redox cycling at the crossing points of the row and column electrodes, electrochemical responses at $n \times n$ crossing points were rapidly detected by using only 2 n bonding pads for the external connection. Based on the detection system, a series of apparatus for biological assay had been developed [23–25]. On the basis of the previous researches [22–25], here, we demonstrate a new amperometric approach for high-throughput detection of DNA hybridization. The principle was based on immobilization and hybridization of DNA inhibited the redox cycling of $Fe(CN)_6^{4-}/Fe(CN)_6^{3-}$ at the designated microwells due to the negatively charged sugar phosphate backbone of DNA [26,27], resulting in decrease of the amperometric signal, and which can be used to assay DNA hybridization. To the best of our knowledge, this is the first report on the amperometric detection of DNA hybridization using this novel multipoint addressable electrochemical device. It is envisioned that this device can be applied to comprehensive and high-throughput detection and imaging of biochemical species.

* Corresponding author at: Advanced Institute of Materials Research, Tohoku University, 2-1-1 Katahira, Aoba, Sendai 980-8579, Japan.
E-mail address: matsue@bioinfo.che.tohoku.ac.jp (T. Matsue).

0925-4005/$ – see front matter.
doi:10.1016/j.snb.2011.09.004

2. Experimental

2.1. Materials

Capture DNA (sequence: 5′-SH-CCAGTGAGCTTCCCGTTCA-3′), target DNA (sequence: 5′-TGAACGGGAAGCTCACTGG-3′) and mismatched probes (sequence: 5′-TTTCCGCTGAGTCCAGATT-3′) were bought from Nihon Gene Research Laboratories Inc. DNA solutions were prepared by dissolving DNA into 30 mM pH 7.4 phosphate buffer solutions (PBS) containing 0.1 M NaCl and 5 mM KCl.

Primer and positive photoresist (S1818) were purchased from Shipley Far East Ltd., Japan. Negative photoresist (SU-8 3005) was bought from Nippon Kayaku Co. Ltd., Japan. $K_4[Fe(CN)_6]$ was bought from Wako Pure Chemical Industries, Ltd. All chemicals were used as received, and solutions were prepared using Milli-Q reagent water (Milli-Q, Millipore, 18.2-MΩ resistivity).

2.2. Microelectrode array fabrication

An electrode array was constructed on a glass substrate using a photolithographic method [22,28]. The glass substrates were consecutively cleaned by ultrasonication in acetone and 2-propanol. A primer and positive photoresist were spin-coated at 3000 rpm for 30 s on the glass substrate, followed by baking at 95 °C for 5 min. Then, the substrate was irradiated with UV light for 13 s through a chromium mask with microelectrode patterns. After developing, Ti, Pd and Au were deposited on the substrate by sputtering to create a Ti/Pd/Au multilayer. The electrode pattern was revealed using a lift-off technique by immersing the electrode substrate in an acetone bath, then the substrate was dried to form an electrode array consisting of four microband electrodes (thickness: 300 nm; width: 100 μm; band interval: 900 μm, each electrode). This microelectrode array can be used as the column or row electrodes array due to the different arrangement.

Then four microwells with 100 μm width, 100 μm length, and 5 μm depth, were further fabricated on each column electrode using SU-8 3005 (thickness: 5 μm) on one microelectrode array; thereby, 16 microwells were fabricated on the column-electrode substrate, as shown in Fig. 1A.

2.3. Immobilization and hybridization of DNA on the sensing array

First, the substrates were cleaned before the measurements. Then, the capture DNA was immobilized in the 16 microwells of the column electrode via an Au–S linkage. The column electrode was rinsed carefully with PBS solution. Different concentrations of target DNA were carefully added into the microwells at each of the four corners by the pipette, and incubated for 2 h in a humidified incubator. After these, 4.0 mM $Fe(CN)_6^{4-}$ solution containing 0.1 M KCl was applied to cover the column electrode surface and filled in every microwell. Then another microelectrode array (worked as row electrode) without assemble of microwells was carefully attached orthogonally on the column-electrode substrate face-to-face with double-sided adhesive paper (thickness, 10 μm; Lintec Co., Japan) in order to assemble the microelectrode/microwell array with microwells arranged at the 16 crossing points. Thus a device is obtained, as shown in Fig. 1B.

2.4. Instrumentation

The detection system is shown in Fig. 2A. Three channels (W1–W3) of a multichannel potentiostat (HA-1010 mM4, Hokuto Denko, Corp., Tokyo, Japan) were used for potential control and current acquisition. The potentiostat was connected to the electrodes by a multiplexer, and the data were controlled and collected by a program developed by LabVIEW through an AD/DA converter (PXI-2529 and PXI-6723, respectively, National Instrument, Austin, TX). An Ag/AgCl and a Pt wire were used as the reference and counter electrodes, respectively.

2.5. Amperometric scanning procedure

The reference and counter electrode were laid near the device, as shown in Fig. 1C. Electrochemical detection was performed as follows: a voltage (V_C = 0.0 V) was applied to all the column electrodes through W1 of the potentiostat. At the same time a different voltage (V_R = 0.6 V) was applied to row electrode 1 (R1) through W3 of the potentiostat for 2 s to precondition the system and stabilize the current, while the other row electrodes (R2–R4) were set at V_C through W1. Then, column electrode 1 (C1) was connected to W2 set at V_C, and the current data were transferred to a PC. This read-out process was sequentially repeated from C1 to C4 with a read-out time interval of 20 ms in each step. All the current responses through W2 were read out, while W1 was used only for potential control. Since all row electrodes were connected to W1 (set at V_C) during the above process, no redox cycling was expected at the crossing points on R2–R4 during scanning. The same measurements were sequentially repeated for the other row electrodes (R2–R4) to address and acquire all the responses at every crossing point. The total detection time for the 16 addressing points was less than 9 s.

3. Results and discussion

3.1. Principle of detection

The principle of multipoint detection of DNA hybridization is shown in Fig. 3(A). When redox compounds showing reversible electrochemical behavior, such as $Fe(CN)_6^{4-}/Fe(CN)_6^{3-}$, are present in the interspaces between the column and row electrodes, redox cycling between the column and row electrodes proceeds only at crossing points set at appropriate potentials, and amplifies the electrochemical signal. The efficiency of the redox cycling is sensitive to the presence of molecules at the electrode surface. DNA hybridization at the electrode surface partially blocks the redox cycling, thereby decreasing the electrochemical responses.

Fig. 3(B) shows the reduction current at column electrodes with a bare surface, with immobilized probe DNA, and with hybridized DNA in a 4.0 mM $Fe(CN)_6^{4-}$ solution. When the potential of the row electrode was stepped from 0.0 V to 0.6 V, redox cycling of $Fe(CN)_6^{4-}/Fe(CN)_6^{3-}$ proceeded between the row and column electrodes. The reduction current of $Fe(CN)_6^{3-}$ at the column electrode increased rapidly after the potential step and soon showed a steady-state. The level of steady-state current became lower when the column electrode was modified with probe DNA (curve b). A further decrease was observed after hybridization (curve c). Formation of the negatively charged sugar phosphate backbone of DNA at the electrode surface reduces the efficiency of redox cycling of $Fe(CN)_6^{4-}/Fe(CN)_6^{3-}$, resulting in a decrease in the current signals, and thereby allowing the detection of specific DNAs.

3.2. Electrochemical imaging and detection

Capture DNA was immobilized in all 16 microwells via a thiol–Au linkage. Then, different concentrations (0.05, 0.1, 0.5, and 1 μM) of target DNA solution were added to the microwells at the four corners (A, B, C and D, respectively), as shown in Fig. 4(A). Because the gap between the row and column electrodes is 10 μm, redox cycling was expected [29] and the reduction current was acquired, and which can amplify the current responses [30]. Fig. 4(B) is the amplified amperometric imaging of the 16 microwells, which clearly shows that the responses at the four corners are

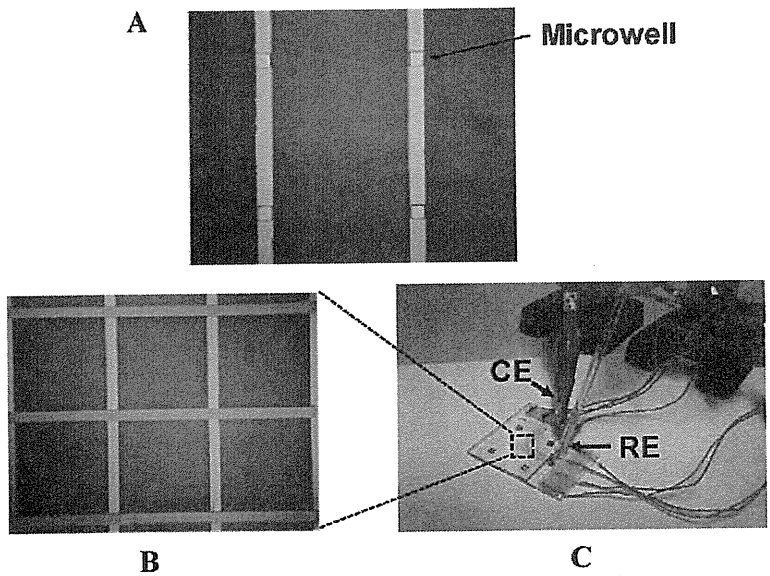

Fig. 1. Optical photographs of (A) the row electrode with microwells, (B) the device consisted of orthogonally arranged arrays of rows and columns of electrodes, and (C) the use of the device with reference electrode (RE) and counter electrode (CE).

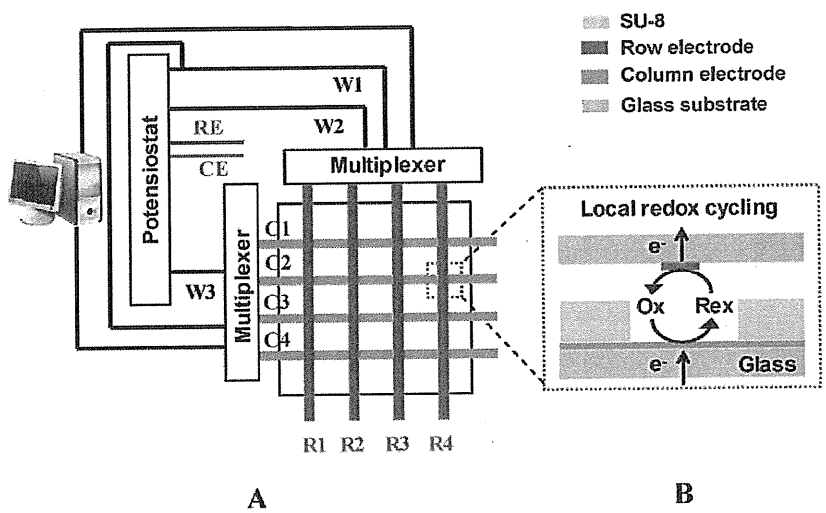

Fig. 2. (A) Schematic diagram of the addressable microelectrode array detection system. The dashed part represents the working area of the device viewed from the top. (B) Side view of a crossing point. Local redox cycling occurs at the crossing points of the column and row electrodes.

lower than those of other areas, indicating that dsDNA efficiently inhibits the redox cycling of $Fe(CN)_6^{4-}/Fe(CN)_6^{3-}$ in the microwells located at the crossing points of the row and column electrodes. It is also found that the response decreases with increasing concentration of target DNA, as shown in Fig. 4(C). The responses show obvious concentration dependence in the range of 0.05 ~ 1 μM. The linear range of this array is wider than the published one [19]. And this DNA array has a detection limit of 0.03 μM (defined as S/N = 3), which is similar to the previous report [31].

3.3. *Specificity and reproducibility of the microelectrode*

We also investigated the influence of a mismatched probe (1 μM, sequence: 5′-TTTCCGCTGAGTCCAGATT-3′). Capture DNA was chemically immobilized by a thiol–Au linkage in eight microwells, then the target DNA or mismatched DNA was added to the designated microwells shown in Fig. 5(A). Fig. 5(B) shows the histogram of the amplified current responses at different crossing points modified with different DNAs. Immobilization of capture DNA in the microwells decreased the current responses, whereas no decrease in the current signal was observed when the target DNA was added into bare microwells. This result indicates that the target DNA does not physically adsorb onto the microwells. A significant decrease in the current responses was observed when the target DNA was introduced into the capture DNA-immobilized microwells. On the other hand, the presence of the mismatched DNA only led to a slight decrease in the current response. The above results demonstrate that this device can be used for multipoint addressable detection of DNAs with well specificity.

Additionally, the untapped devices are used to repeat above modified process (immobilization and hybridization of DNA) and electrochemical experiment. It is found that current responses in each microwells changed ±4%. And after the repeated measurement (10 times), the current responses kept about 95%, which shows this DNA array has well reproducibility and stability.

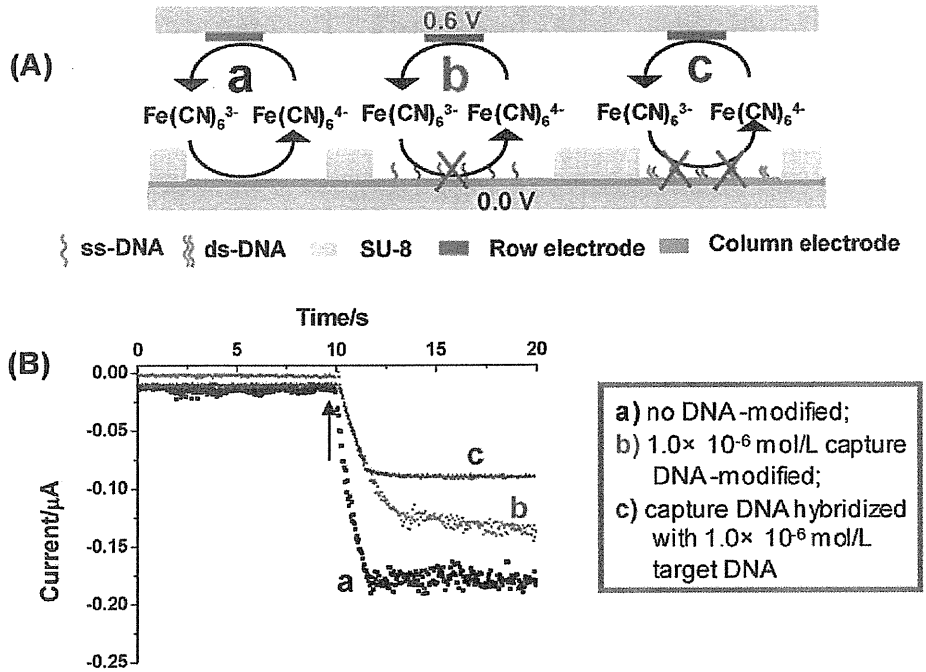

Fig. 3. (A) Principle of multipoint detection of DNA hybridization. (B) Amperometric responses at different gold microelectrodes; curves a, b, and c are the bare gold microelectrode, the ssDNA-modified, and the dsDNA-modified microelectrode, respectively. The potential of the row electrode was stepped from 0.0 V to 0.6 V at the point indicated by the arrow.

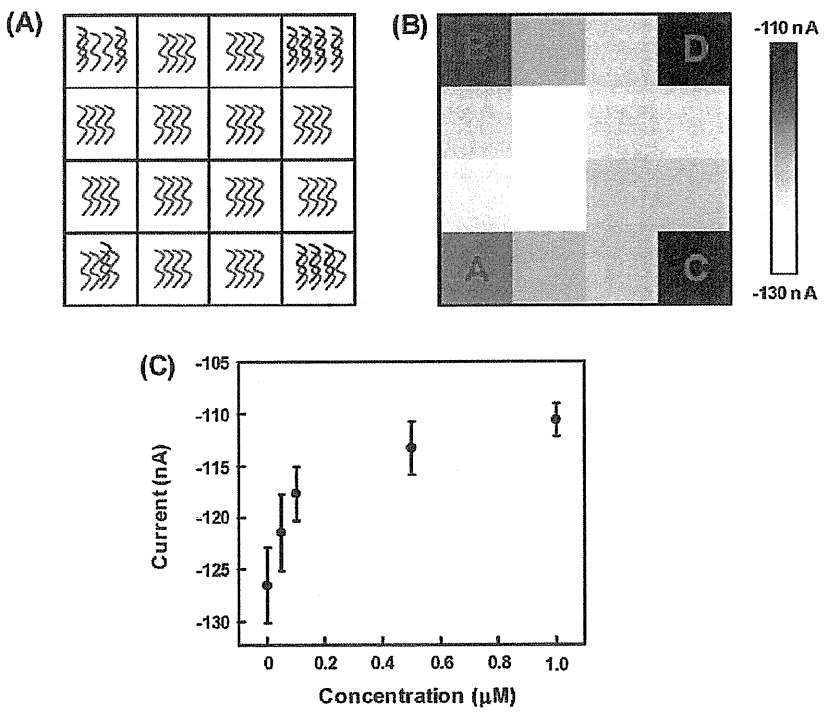

Fig. 4. Detection of DNA hybridization. (A) Schematic of the modification of DNA, and (B) imaging of the amplified reduction current responses at the 16 crossing points. The capture probes were modified at all crossing points, and different concentrations (0.05, 0.1, 0.5, and 1 μM) of target DNA were modified at the four corners (A, B, C, and D, respectively). (C) The relationship between different concentrations of target DNA and reduction currents. Data points represent means ± SD of three independent experiments.

3.4. Prospect of this device

Based on above results, it is envisioned that this device has applications in high-throughput DNA assays, such as DNA diagnostics, gene analysis, fast detection of biological warfare agents, and forensic applications. For example, it can be used to simultaneous detection of the HIV-1 and HIV-2 oligonucleotides [19] and different food-contaminating pathogenic bacteria [20].

Although the present method is suitable for high-throughput DNA assays, the present method may be unsuitable for highly

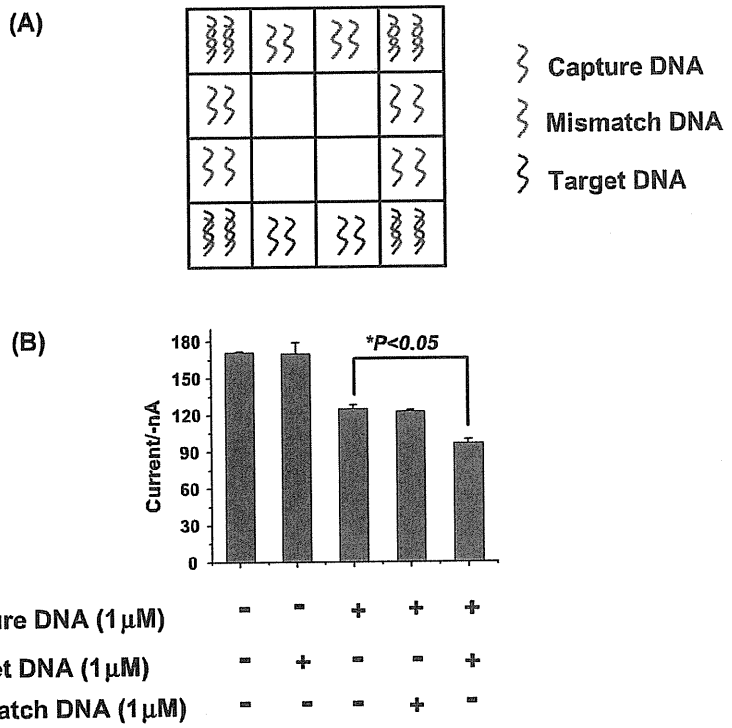

Fig. 5. (A) Schematic diagram of the crossing points modified with different DNAs. (B) Histogram of the amplified reduction current responses at different crossing points modified with different DNAs. The columns from left to right are the currents of the microwells without DNA, with modified-target DNA, with modified-capture DNA, with modified-(capture DNA + mismatched DNA), and with modified-(capture DNA + target DNA). The concentrations of capture DNA, target DNA, and mismatched DNA were 1 μM. Data points represent means ± SD of three independent experiments.

sensitive DNA detection (e.g. detection of DNA in blood) because the sensitivity of the present device is not very high compared to that of conventional methods (e.g. fluorescence and PCR methods). We think that this kind of device can be used for a simple test for a sample with large amounts of DNA fragments. It is necessary to improve the sensitivity for a detailed analysis. It is important for improving the sensitivity of the assay to reduce the gap between the row electrode and column electrode and to amplify electrochemical signals. Wolfrum et al. have reported over 1000-fold electrochemical signal amplification based on rapid redox cycling between plane parallel electrodes inside a nanochannel (height, 55 nm) [32]. Therefore, it is expected to amplify significantly electrochemical signals by reducing the gap between the row electrode and column electrode of the present device.

4. Conclusions

We have devised a high-throughput amperometric DNA assay using a novel addressable electrochemical device. Immobilization and hybridization of DNA in microwells decrease the amperometric responses from redox cycling at the crossing points of row and column electrodes. The observed current decrease demonstrates that we have successfully performed multipoint, and addressable detection of target DNA. Additionally, this device has good selectivity to specific DNA. This methodology will afford an inexpensive platform for comprehensive, high-throughput assays in clinical diagnosis.

Acknowledgments

This study was partly supported by the Formation of Innovation Center for Fusion of Advanced Technologies, Special Coordination Funds for Promoting Science and Technology, and by Grant-in-Aid for Scientific Research (22245011) from the Ministry of Education, Culture, Sports, Science and Technology, Japan. This study was also supported by the CASIO Science Promotion Foundation. We also thank the National Nature Sciences Funding of China for their support (20735002, 41076059 and 20905013).

References

[1] J. Lamartine, Materials Science and Engineering C 26 (2006) 354–359.
[2] F. Bertucci, R. Houlgatte, C. Nguyen, P. Viens, B. Jordan, D. Birnbaum, The Lancet Oncology 2 (2001) 674–682.
[3] P. Bryant, D. Venter, R. Robinsbrowne, N. Curtis, The Lancet Infectious Diseases 4 (2004) 100–111.
[4] C.C. Xiang, Y. Chen, Biotechnology Advances 18 (2000) 35–46.
[5] J.M. Moran-Mirabal, C.P. Tan, R.N. Orth, E.O. Williams, H.G. Craighead, D.M. Lin, Analytical Chemistry 79 (2007) 1109–1114.
[6] K.D. Barbee, X. Huang, Analytical Chemistry 80 (2008) 2149–2154.
[7] J. Kim, R.M. Crooks, Analytical Chemistry 79 (2007) 7267–7274.
[8] F.J. Steemers, J.A. Ferguson, D.R. Walt, Nature Biotechnology 18 (2000) 91–94.
[9] H.A. Behrensdorf, M. Pignot, N. Windhab, A. Kappel, Nucleic Acids Research 30 (2002) e64.
[10] J.R. Epstein, A.P.K. Leung, K.-H. Lee, D.R. Walt, Biosensors and Bioelectronics 18 (2003) 541–546.
[11] S.J. Lassiter, W.J. Stryjewski, Y. Wang, S.A. Soper, Spectroscopy 17 (2002) 14–23.
[12] S.-J. Park, T.A. Taton, C.A. Mirkin, Science 295 (2002) 1503–1506.
[13] A. Sassolas, B.D. Leca-Bouvier, L.J. Blum, Chemical Reviews 108 (2008) 109–139.
[14] Y. Huang, K.L. Ewalt, M. Tirado, R. Haigis, A. Forster, D. Ackley, M.J. Heller, J.P. O'Connell, M. Krihak, Analytical Chemistry 73 (2001) 1549–1559.
[15] D. Xu, D. Xu, X. Yu, Z. Liu, W. He, Z. Ma, Analytical Chemistry 77 (2005) 5107–5113.
[16] L. Niu, W. Knoll, Analytical Chemistry 79 (2007) 2695–2702.
[17] H. Li, Z. Sun, W. Zhong, N. Hao, D. Xu, H.-Y. Chen, Analytical Chemistry 82 (2010) 5477–5483.
[18] R. Kalantari, R. Cantor, H. Chen, G. Yu, J. Janata, M. Josowicz, Analytical Chemistry 82 (2010) 9028–9033.
[19] D. Zhang, Y. Peng, H. Qi, Q. Gao, C. Zhang, Biosensors and Bioelectronics 25 (2010) 1088–1094.
[20] F. Farabullini, F. Lucarelli, I. Palchetti, G. Marrazza, M. Mascini, Biosensors and Bioelectronics 22 (2007) 1544–1549.
[21] Y.-S. Choi, K.-S. Lee, D.-H. Park, Journal of Micromechanics Microengineering 15 (2005) 1938–1946.
[22] Z. Lin, Y. Takahashi, Y. Kitagawa, T. Umemura, H. Shiku, T. Matsue, Analytical Chemistry 80 (2008) 6830–6833.
[23] Z. Lin, Y. Takahashi, T. Murata, M. Takeda, K. Ino, H. Shiku, T. Matsue, Angewandte Chemie International Edition 48 (2009) 2044–2046.

[24] Z. Lin, K. Ino, H. Shiku, T. Matsue, Chemical Communications 46 (2010) 559–561.
[25] Z. Lin, K. Ino, H. Shiku, T. Matsue, G. Chen, Chemical Communications 46 (2010) 243–245.
[26] B. Lillis, M. Manning, E. Hurley, H. Berney, R. Duane, A. Mathewson, M.M. Sheehan, Biosensors and Bioelectronics 22 (2007) 1289–1295.
[27] H. Peng, C. Soeller, N.A. Vigar, V. Caprio, J. Travas-Sejdic, Biosensors and Bioelectronics 22 (2007) 1868–1873.
[28] K. Ino, H. Shiku, F. Ozawa, T. Yasukawa, T. Matsue, Biotechnology and Bioengineering (2009) 709–718.
[29] S.K. Kim, P.J. Hesketh, C. Li, J.H. Thomas, H.B. Halsall, W.R. Heineman, Biosensors and Bioelectronics 20 (2004) 887–894.
[30] T. Yasukawa, K. Nagamine, Y. Horiguchi, H. Shiku, M. Koide, T. Itayama, F. Shiraishi, T. Matsue, Analytical Chemistry 80 (2008) 3722–3727.
[31] O.Y.F. Henry, J.L. Acero Sanchez, D. Latta, C.K. O'Sullivan, Biosensors and Bioelectronics 24 (2009) 2064–2070.
[32] B. Wolfrum, M. Zevenbergen, S. Lemay, Analytical Chemistry 80 (2008) 972–977.

Biographies

Xi Zhu received his BS degree in 2006 from Fujian Normal University, China. Currently, he is studying for the degree of PhD in Fuzhou University, China.

Kosuke Ino received his PhD degree in Engineering from Nagoya University in 2008. He received Research Fellow of the Japan Society for the Promotion of Science (2006–2008). He is currently working as an assistant professor in Graduate School of Environmental Studies, Tohoku University.

Zhenyu Lin received his PhD in analytical chemistry from Fuzhou University in 2007. He is currently working as an associate professor in Department of Chemistry, Fuzhou University.

Hitoshi Shiku received his PhD in Engineering from the Tohoku University in 1997. He is currently working as an associate professor in Graduate School of Environmental Studies, Tohoku University.

Guonan Chen received his BS degree and MS degree from Fuzhou University, China in 1975 and 1982, respectively, and received his PhD from LA TROBE University, Australia in 1990. He is currently a professor in Fuzhou University, China.

Tomokazu Matsue received his PhD in pharmacy from Tohoku University in 1981. He is currently working as a professor in Advanced Institute of Materials Research (WPI-AIMR) and an adjunct professor in Graduate School of Environmental Studies, Tohoku University.

Growth differentiation factor 3 is induced by bone morphogenetic protein 6 (BMP-6) and BMP-7 and increases luteinizing hormone receptor messenger RNA expression in human granulosa cells

Jia Shi, M.D., Ph.D., Osamu Yoshino, M.D., Ph.D., Yutaka Osuga, M.D., Ph.D., Ikumi Akiyama, M.D., Miyuki Harada, M.D., Ph.D., Kaori Koga, M.D., Ph.D., Akihisa Fujimoto, M.D., Ph.D., Tetsu Yano, M.D., Ph.D., and Yuji Taketani, M.D., Ph.D.

Department of Obstetrics and Gynecology, University of Tokyo, Tokyo, Japan

Objective: To examine the relevance of growth differentiation factor 3 (GDF-3) and bone morphogenetic protein (BMP) cytokines in human ovary.
Design: Molecular studies.
Setting: Research laboratory.
Patient(s): Eight women undergoing salpingo-oophorectomy and 30 women undergoing ovarian stimulation for in vitro fertilization.
Intervention(s): Localizing GDF-3 protein in human ovaries; granulosa cells (GC) cultured with GDF-3, BMP-6, or BMP-7 followed by RNA extraction.
Main Outcome Measure(s): The localization of GDF-3 protein in normal human ovaries via immunohistochemical analysis, GDF-3 messenger RNA (mRNA) expression evaluation via quantitative real-time reverse transcription and polymerase chain reaction (RT-PCR), and evaluation of the effect of GDF-3 on leuteinizing hormone (LH) receptor mRNA expression via quantitative real-time RT-PCR.
Result(s): In the ovary, BMP cytokines, of the transforming growth factor beta (TGF-β) superfamily, are known as a luteinization inhibitor by suppressing LH receptor expression in GC. Growth differentiation factor 3, a TGF-β superfamily cytokine, is recognized as an inhibitor of BMP cytokines in other cells. Immunohistochemical analysis showed that GDF-3 was strongly detected in the GC of antral follicles. An in vitro assay revealed that BMP-6 or BMP-7 induced GDF-3 mRNA in GC. Also, GDF-3 increased LH receptor mRNA expression and inhibited the effect of BMP-7, which suppressed the LH receptor mRNA expression in GC.
Conclusion(s): GDF-3, induced with BMP-6 and BMP-7, might play a role in folliculogenesis by inhibiting the effect of BMP cytokines. (Fertil Steril® 2012;97:979–83. ©2012 by American Society for Reproductive Medicine.)
Key Words: BMP, GDF-3, LH receptor, ovary

Follicular growth, selection, and ovulation are essential processes for the achievement of pregnancy. Once follicle growth progresses beyond the secondary stage, granulosa cells (GC) express follicle-stimulating hormone (FSH) receptor and proliferate under the stimulation of FSH (1). When the follicle approaches ovulation, luteinizing hormone (LH) receptor is increasingly expressed in GC. The increase in LH receptors makes GC sensitive to the LH surge that cues luteinization of these cells. Any perturbation of these events, such as premature luteinization or luteinization failure, has the potential to impair reproduction (2, 3).

Bone morphogenetic protein (BMP) cytokines, members of the transforming growth factor beta (TGF-β) superfamily, are required for follicular growth in many species. Oocytes express BMP-6 and BMP-15 and growth differentiation factor 9 (GDF-9); GC express BMP-2 and BMP-6; and theca cells express BMP-4 and BMP-7 (4, 5). The BMP cytokines contribute to folliculogenesis by inhibiting premature luteinization

Received November 11, 2011; revised January 1, 2012; accepted January 10, 2012; published online February 1, 2012.
J.S. has nothing to disclose. O.Y. has nothing to disclose. Y.O. has nothing to disclose. I.A. has nothing to disclose. M.H. has nothing to disclose. K.K. has nothing to disclose. A.F. has nothing to disclose. T.Y. has nothing to disclose. Y.T. has nothing to disclose.
Supported by Health and Labor Sciences Research Grants from the Ministry of Health, Labor and Welfare of Japan, and a Grant-in-Aid for Scientific Research from the Ministry of Education, Culture, Sports, Science and Technology.
Reprint requests: Osamu Yoshino, M.D., Ph.D., Department of Obstetrics and Gynecology, University of Tokyo, Tokyo (E-mail: oyoshino624@hotmail.co.jp).

Fertility and Sterility® Vol. 97, No. 4, April 2012 0015-0282/$36.00

doi:10.1016/j.fertnstert.2012.01.100

by suppressing LH receptors (4). It is interesting that mice or sheep with abnormalities in BMP signaling exhibit a precocious maturation of ovarian follicles (2–4). In conditional knockout mice against SMAD-4, which is a necessary factor for TGF-β ligand signaling, GC express a higher amount of LH receptors (3). Therefore, malfunction of the BMP cytokines, which inhibit premature luteinization by suppressing the LH receptor, may lead to inadequate follicular development and impaired fertility (4).

In normal ovaries, follicles still possess BMP cytokines in granulosa and theca cells as late as the preovulatory stage (4, 6, 7). Therefore, it is plausible that some mechanisms exist to suppress the antiluteinizing effect of BMP cytokines, especially in preovulatory follicles. But the precise mechanisms remain to be elucidated.

Growth differentiation factor 3, a member of TGF-β superfamily, is known to inhibit BMP cytokines in frog embryos (8, 9), human embryonic stem (ES) cells (9, 10), and mouse ES cells (9). In ES cells, GDF-3 inhibits BMP cytokines' signaling to maintain pluripotency of cells (9, 10). However, the role of GDF-3 in the ovary is still unclear. We hypothesized that GDF-3 might inhibit the effect of BMP cytokines, which are known as a luteinization inhibitor, to lead to follicular maturation. We investigated the localization of GDF-3 in the human ovary and examined its function, especially from the point of LH receptor mRNA expression in GC.

MATERIALS AND METHODS

The experimental procedures were approved by the institutional review board, and signed, informed consent for use of the samples was obtained from each patient. Except where otherwise indicated, all reagents were purchased from Sigma. Recombinant human GDF-3 and BMP-7 were purchased from R&D Systems. An antibody against GDF-3 was purchased from Lifespan Biosciences.

Collection of Ovarian Tissues and Immunohistochemistry

Tissue specimens of human ovaries were obtained after signed, informed consent from eight women (age range: 28 to 40 years) who underwent salpingo-oophorectomy for the treatment of uterine cervical cancer. All patients had normal ovarian cycles before surgery, and no histologic abnormalities or malignant lesions were observed in the ovarian tissues. Ovarian tissues were fixed in neutral-buffered formalin and embedded in paraffin blocks, and 6-μm sections were prepared. Antigen retrieval was performed using sodium citrate buffer (10 mM, pH 6.0) (11). The sections were stained with 10 μg/mL anti-GDF-3 antibody or rabbit IgG as a negative control by use of an Envision+ System/HRP rabbit kit (DAB+; Dako Japan). In some experiments, GDF-3 antibody, which had been preabsorbed with recombinant GDF-3 (50 μg/mL), was used as a preabsorption control.

Cell Culture of Human Granulosa Cells (GC)

Granulosa cells were obtained from 30 patients undergoing ovarian stimulation for in vitro fertilization (IVF). The method to purify and culture human GC was described previously elsewhere (12). The collected human GC were cultured in Dulbecco's modified eagle medium/nutrient mixture F-12 (DMEM/F-12) containing 5% fetal bovine serum (FBS) and antibiotics in 12-well plates at a density of 2×10^5 cells/mL. To investigate the regulation of GDF-3, GC were cultured with BMP-6 (100 ng/mL) or BMP-7 (100 ng/mL) for 24 hours. To evaluate the effects of GDF-3, human GC were cultured with or without GDF-3 (60–100 ng/mL) for 24 hours in the presence or absence of BMP-7 (10–100 ng/mL). The GDF-3 was used 30 minutes before stimulation with BMP-7.

Reverse Transcription (RT) and Quantitative Real-Time Polymerase Chain Reaction (PCR) Analysis

Total RNA was extracted from GC by use of the RNeasy mini-kit (Qiagen). Reverse transcription (RT) was performed using Rever Tra Dash (Toyobo). One microgram of total RNA was reverse transcribed in a 20-μL volume. For the quantification of various mRNA levels, real-time polymerase chain reaction (PCR) was performed using a LightCycler (Roche Diagnostic GmbH), according to the manufacturer's instructions. The PCR primers were selected from different exons of the corresponding genes to discriminate the PCR products that might arise from possible chromosomal DNA contaminants. The primer sequences and real-time PCR conditions were previously described elsewhere (12), with the exception of the primer sequence of GDF-3 (NM_020634: 152-171 and 410-391). Relative expression of each mRNA was normalized by glyceraldehyde 3-phosphate dehydrogenase (GAPDH) mRNA. All results were shown as mean $\pm$ standard deviation (SD) of data from at least three separate experiments. Data were analyzed by one-way analysis of variance (ANOVA) with post hoc test for multiple comparisons. $P<.05$ was considered statistically significant.

RESULTS

The Localization of GDF-3 in Human Ovaries

The localization of GDF-3 protein in human ovaries was examined by immunohistochemistry using normal human ovaries. The intensity of the staining of GDF-3 in GC was negative in primordial and primary follicles; and weak in GC of secondary follicles (Fig. 1A, 1C, and 1D), while GDF-3 protein was detected in the oocytes of primordial, primary, and secondary follicles. As shown in Figure 1E and G, GDF-3 was strongly detected in the GC of antral follicles. With preabsorption GDF-3 antibody, which had been preabsorbed with recombinant GDF-3, the intensity was decreased (see Fig. 1I).

Regulation of GDF-3 in GC

To investigate the regulation of GDF-3 gene expression, human GC were cultured with BMP-6 or BMP-7. As shown in Figure 2, there was an approximately fourfold to fivefold ($n = 5$, $P<.01$) increase in GDF-3 mRNA expression with BMP-6 or BMP-7 stimulation compared with control samples.

FIGURE 1

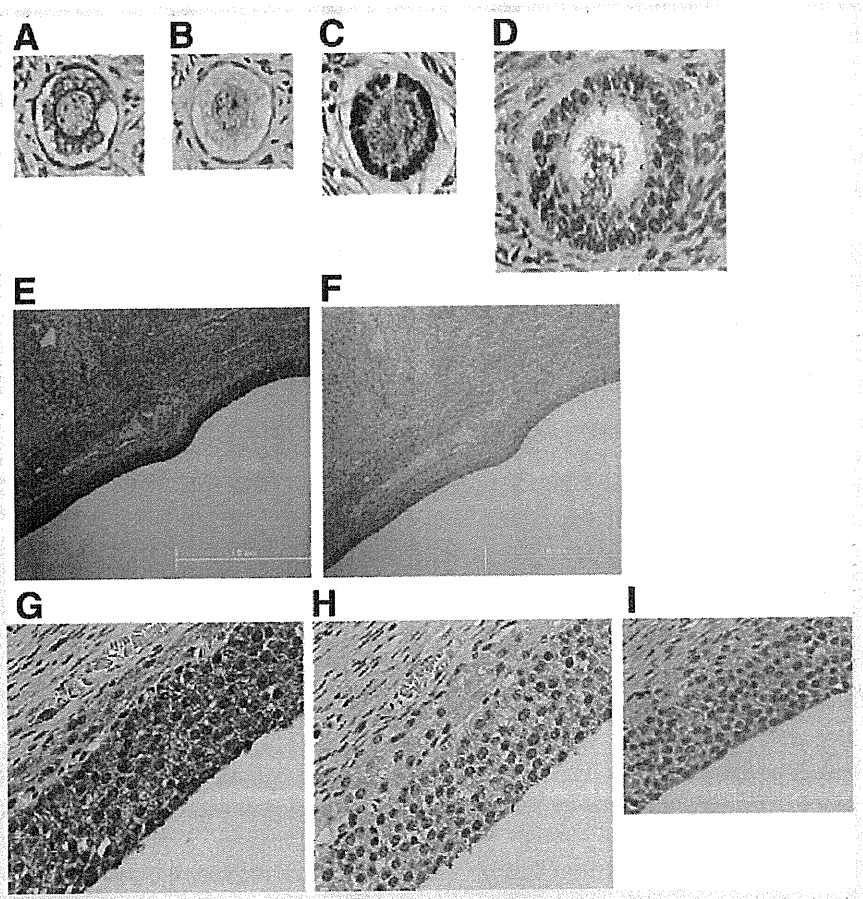

Immunohistochemistry of growth differentiation factor (GDF)-3 in human ovary. GDF-3 protein localization was examined in normal human ovaries. Ovarian tissues were fixed in neutral-buffered formalin and embedded in paraffin blocks. The sections were stained with 10 μg/mL anti-GDF-3 antibody or rabbit IgG as negative control. GDF-3 antibody, which had been preabsorbed with recombinant GDF-3, was also used as a preabsorption control. Representative data from eight specimens were shown. (A, B) Primordial follicle. (C) Primary follicle. (D) Secondary follicle. (E–I) Antral follicle. A, C, D, E, G: Anti-GDF-3 antibody. B, F, H: Negative control antibody. I: GDF-3 antibody, which had been preabsorbed with recombinant GDF-3, was used as a preabsorption control. E, F: lower magnification, ×40. A–D, G–I: higher magnification, ×200.

Shi. Role of GDF-3 in human ovary. Fertil Steril 2012.

The Effect of GDF-3 on Gene Expression of Folliculogenesis Factors

As shown in Figure 3, in the absence of BMP-7, GDF-3 (0–100 ng/mL) increased the expression of LH receptor mRNA. As previously reported elsewhere (12), BMP-7 (10–100 ng/mL) stimulation for 24 hours statistically significantly decreased the gene expression of LH receptor in human GC. Also, GDF-3 inhibited the effect of BMP-7 in suppressing LH receptor mRNA ($P<.01$), and the same tendency was found when BMP-7 was substituted for BMP-6 (data not shown).

DISCUSSION

Growth differentiation factor 3 is a member of the TGF-β superfamily, and its expression has been reported in undifferentiated ES cells (9, 10), white adipose tissue (13), and the brain (14). Functionally, GDF-3 is known to inhibit the effect of BMP cytokines. In human ES cells, inhibition of BMP-2 signaling by GDF-3 maintains pluripotency (10). Furthermore, induction of GDF-3 in frog embryos impairs the effect of BMP cytokines, enabling secondary axis induction and direct neural induction of embryos (8, 9).

Although the expression of GDF-3 mRNA in the human ovary had been demonstrated via RT-PCR (15), its localization and regulation remained to be elucidated. Our immunohistochemical study revealed that, in GC, GDF-3 protein was localized in GC of antral follicles, while GDF-3 staining was negative or weak in preantral follicles. We also observed strong staining levels of GDF-3 protein in the oocytes of primordial and primary follicles. We also have demonstrated that BMP-6 and BMP-7 statistically significantly induced GDF-3 mRNA in human GC. In the ovary, BMP-6 is derived from oocytes and GC, while BMP-7 originates in theca cells (5). Thus, an autocrine or paracrine mechanism might be working on GC to regulate GDF-3 expression in the follicles.

Next, we examined the role of GDF-3 in human GC and found that GDF-3 increased the expression of LH receptor mRNA (see Fig. 3). Granulosa cells are known to express

FIGURE 2

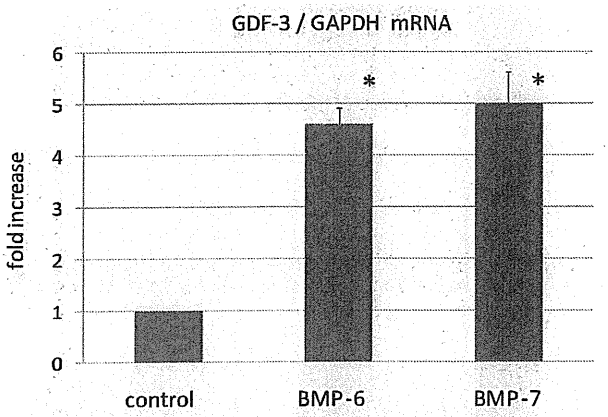

Effect of bone morphogenetic protein 6 (BMP-6) and BMP-7 on growth differentiation factor 3 (GDF-3) mRNA expression. Human granulosa cells (GC) were cultured with BMP-6 or BMP-7 for 24 hours. The concentration of BMP cytokines was 100 ng/mL. Total RNA was extracted from the GC and subjected to quantitative real-time polymerase chain reaction (PCR) to determine GDF-3 mRNA levels. Data were normalized to glyceraldehyde 3-phosphate dehydrogenase (GAPDH) mRNA levels. Representative data from three different experiments was shown as the mean ± standard deviation (SD) relative to an adjusted value of 1.0 for the mean value of the each control. *$P<.01$ versus control.

Shi. Role of GDF-3 in human ovary. Fertil Steril 2012.

FIGURE 3

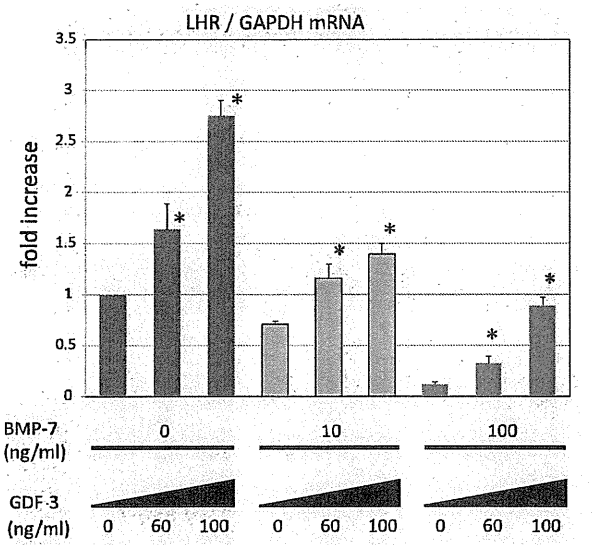

Effect of growth differentiation factor 3 (GDF-3) on luteinizing hormone (LH) receptor mRNA expression. Human granulosa cells (GC) were cultured with GDF-3 (60–100 ng/mL) in the presence or absence of bone morphogenetic protein 7 (BMP-7) (10–100 ng/mL) for 24 hours. GDF-3 was added 30 minutes before BMP-7 incubation. Total RNA was extracted from the GC and subjected to quantitative real-time polymerase chain reaction (PCR) to determine the LH receptor mRNA levels. Data were normalized to glyceraldehyde 3-phosphate dehydrogenase (GAPDH) mRNA levels. Representative data from three different experiments was shown as the mean ± standard deviation (SD) relative to an adjusted value of 1.0 for the mean value of the each control. *$P<.05$ versus control.

Shi. Role of GDF-3 in human ovary. Fertil Steril 2012.

BMP-2 and BMP-6, which have the potential to suppress LH receptor mRNA expression (6, 7). Also, GDF-3 exhibits its inhibitory effect on BMP cytokines by via extracellular binding of the cytokines (9). Therefore, GDF-3 might increase LH receptor mRNA expression by blocking the effect of BMP-2 and/or BMP-6, which are derived from GC (6, 7). As previously reported elsewhere (12), we found that BMP-7 suppressed LH receptor mRNA expression in a dose-dependent manner, and that GDF-3 inhibited the effect of BMP-7 in suppressing LH receptor mRNA expression (see Fig. 3).

During the process of follicular growth, the expression of BMP-2 and BMP-6 in GC and that of BMP-4 and BMP-7 in theca cells increases in rats (4) and humans (6, 7). These BMP cytokines are known to suppress the LH receptor, which is a key factor in the luteinization process (4). Therefore, these BMP cytokines may contribute to folliculogenesis by preventing precocious maturation of ovarian follicles. Abnormal BMP signaling in vivo leads to a precocious maturation of ovarian follicles (2, 3), which is consistent with this theory. However, before ovulation, the LH receptor expression must be induced in GC for follicles to respond to the LH surge. Thus, the function of BMP cytokines must be blocked in the preovulatory phase. Our present findings have revealed that GDF-3, which was induced with BMP stimulation and expressed mainly in antral follicles, might play a role as a BMP inhibitor.

Fine-tuning of BMP expression levels might lead to the appropriate transition from the growing follicle to the preovulatory follicle. We also found GDF-3 protein localization in oocytes of growing follicles. As oocytes express various BMP cytokines (4), GDF-3 might work as a negative regulator of oocyte-derived BMP cytokines in the growing follicle. The role of GDF-3 in the human oocyte remains to be elucidated.

Acknowledgments: The authors thank Dr. Heather M. Martinez for her helpful discussion and critical reading of the manuscript.

REFERENCES

1. Minegishi T, Tano M, Igarashi M, Rokukawa S, Abe Y, Ibuki Y, et al. Expression of follicle-stimulating hormone receptor in human ovary. Eur J Clin Invest 1997;27:469–74.
2. McNatty KP, Henderson KM. Gonadotrophins, fecundity genes and ovarian follicular function. J Steroid Biochem 1987;27:365–73.
3. Pangas SA, Li X, Robertson EJ, Matzuk MM. Premature luteinization and cumulus cell defects in ovarian-specific Smad4 knockout mice. Mol Endocrinol 2006;20:1406–22.
4. Shimasaki S, Moore RK, Otsuka F, Erickson GF. The bone morphogenetic protein system in mammalian reproduction. Endocr Rev 2004;25:72–101.
5. Knight PG, Glister C. TGF-beta superfamily members and ovarian follicle development. Reproduction 2006;132:191–206.
6. Shi J, Yoshino O, Osuga Y, Koga K, Hirota Y, Hirata T, et al. Bone morphogenetic protein-6 stimulates gene expression of follicle-stimulating hormone receptor, inhibin/activin beta subunits, and anti-müllerian hormone in human granulosa cells. Fertil Steril 2009;92:1794–8.

7. Shi J, Yoshino O, Osuga Y, Koga K, Hirota Y, Nose E, et al. Bone morphogenetic protein-2 (BMP-2) increases gene expression of FSH receptor and aromatase and decreases gene expression of LH receptor and StAR in human granulosa cells. Am J Reprod Immunol 2011;65:421–7.
8. Levine AJ, Levine ZJ, Brivanlou AH. GDF3 is a BMP inhibitor that can activate nodal signaling only at very high doses. Dev Biol 2009;325: 43–8.
9. Levine AJ, Brivanlou AH. GDF3, a BMP inhibitor, regulates cell fate in stem cells and early embryos. Development 2006;133:209–16.
10. Peerani R, Rao BM, Bauwens C, Yin T, Wood GA, Nagy A, et al. Niche-mediated control of human embryonic stem cell self-renewal and differentiation. EMBO J 2007;26:4744–55.
11. Shi SR, Chaiwun B, Young L, Cote RJ, Taylor CR. Antigen retrieval technique utilizing citrate buffer or urea solution for immunohistochemical demonstration of androgen receptor in formalin-fixed paraffin sections. J Histochem Cytochem 1993;41:1599–604.
12. Shi J, Yoshino O, Osuga Y, Nishii O, Yano T, Taketani Y. Bone morphogenetic protein 7 (BMP-7) increases the expression of follicle-stimulating hormone (FSH) receptor in human granulosa cells. Fertil Steril 2010;93:1273–9.
13. Witthuhn BA, Bernlohr DA. Upregulation of bone morphogenetic protein GDF-3/Vgr-2 expression in adipose tissue of FABP4/aP2 null mice. Cytokine 2001;14:129–35.
14. Hexige S, Guo J, Ma L, Sun Y, Liu X, Yan X, et al. Expression pattern of growth/differentiation factor 3 in human and murine cerebral cortex, hippocampus as well as cerebellum. Neurosci Lett 2005;389:83–7.
15. Clark AT, Rodriguez RT, Bodnar MS, Abeyta MJ, Cedars MI, Turek PJ, et al. Human STELLAR, NANOG, and GDF3 genes are expressed in pluripotent cells and map to chromosome 12p13, a hotspot for teratocarcinoma. Stem Cells 2004;22:169–79.

ELSEVIER

THE JOURNAL OF
MINIMALLY INVASIVE
GYNECOLOGY

Original Article

Myomectomy Decreases Abnormal Uterine Peristalsis and Increases Pregnancy Rate

Osamu Yoshino, MD, PhD*, Osamu Nishii, MD, PhD, Yutaka Osuga, MD, PhD, Hisanori Asada, MD, PhD, Shigeo Okuda, MD, PhD, Makoto Orisaka, MD, PhD, Masaaki Hori, MD, PhD, Toshihiro Fujiwara, MD, PhD, and Toshihiko Hayashi, MD, PhD

From the Department of Obstetrics and Gynecology, University of Tokyo (Drs. Yoshino and Osuga), Department of Obstetrics and Gynecology (Dr. Asada), Department of Radiology, Keio University (Dr. Okuda), Department of Radiology, Juntendo University (Dr. Hori), Reproduction Center, Sanno Hospital (Dr. Fujiwara), Tokyo, Departments of Obstetrics and Gynecology (Drs. Yoshino and Nishii), Radiology (Dr. Hayashi), Mizonokuchi Hospital, Teikyo University, Kanagawa, and Department of Obstetrics and Gynecology, University of Fukui (Dr. Orisaka), Fukui, Japan.

ABSTRACT **Background:** The relationship between fibroids and infertility remains a critical and unresolved question. During the implantation phase, it is known that uterine peristalsis is dramatically reduced, which is thought to facilitate implantation of the embryo to the endometrium. In the previous study, using a cine MRI mode, we found that less than half of the patients with intramural fibroids exhibited abnormal uterine peristalsis during the mid-luteal phase. In the present study, we further investigated whether myomectomy for patients in the high peristalsis group is a constructive method to normalize uterine peristalsis.
Methods: The frequency of junctional zone movement was evaluated using a cine MRI mode during the mid-luteal phase. Fifteen infertility patients, who had intramural myomas and exhibited abnormal uterine peristalsis ($\geq$2 times/3 min) in their first MRI, underwent myomectomy and a second MRI. After receiving the second MRI, patients underwent infertility treatment for at least 8 months, and pregnancy rate was evaluated prospectively.
Results: Among 15 patients, the frequency of uterine peristalsis was normalized (0 or 1 time/3min) in 14 patients. Following myomectomy and second MRI test, 6 of the 15 patients achieved pregnancy (n = 15, pregnancy rate: 40%).
Conclusions: The presence of uterine fibroids might induce abnormal uterine peristalsis in some patients, leading to infertility, and myomectomy may improve fertility in these patients. Journal of Minimally Invasive Gynecology (2012) 19, 63–67

Keywords: Uterine fibroma; Cine MRI; Uterine peristalsis; Infertility; Myomectomy

DISCUSS You can discuss this article with its authors and with other AAGL members at **http://www.AAGL.org/jmig-19-1-11-00328**

Use your Smartphone to scan this QR code and connect to the discussion forum for this article now*

* Download a free QR Code scanner by searching for "QR scanner" in your smartphone's app store or app marketplace.

The relationship between myomas and infertility remains a critical and unresolved question. Uterine myomas are grouped according to location: submucous, intramural, or subserosal. It is generally accepted that the anatomic location of a uterine myoma is an important factor in determining a patient's course of treatment [1]. Meta-analyses have consistently demonstrated a detrimental effect of submucosal, but not subserosal, myomas on treatment outcomes. However, conclusions regarding intramural myomas are conflicting [1,2]. Moreover, because the pregnancy rate after myomectomy of intramural myomas has varied widely among previous studies, firm conclusions on the significance of myomectomy on fertility cannot be drawn [2]. Therefore management of intramural type myomas continues to be difficult. To address this problem, we focused on the mechanisms through which intramural myomas may influence fertility. It is believed that myomas might interfere

Supported by Health and Labor Sciences Research Grants from the Ministry of Health, Labor and Welfare of Japan, Grant-in-Aid for Scientific Research from the Ministry of Education, Culture, Sports, Science and Technology.
The authors have no commercial, proprietary, or financial interest in the products or companies described in this article.
Corresponding author: Osamu Yoshino, MD, PhD, University of Tokyo, Department of Obstetrics and Gynecology, 7-3-1 Hongo, Bunkyo-ku, Tokyo 113-8655, Japan.
E-mail: oyoshino624@hotmail.co.jp

Submitted July 8, 2011. Accepted for publication September 21, 2011.
Available at www.sciencedirect.com and www.jmig.org

1553-4650/$ - see front matter
doi:10.1016/j.jmig.2011.09.010

with the process of embryo implantation [3]. This detrimental effect on implantation may be mediated by the occurrence of abnormal uterine contractility [2,4].

During the implantation phase, it is known that uterine peristalsis is dramatically reduced, which is believed to facilitate implantation of the embryo to the endometrium. In a previous study, we examined the frequency of uterine peristalsis with a cine magnetic resonance imaging (MRI) mode display [5]. Among 51 patients with infertility harboring intramural myomas, 22 patients (43%) exhibited a high frequency of uterine peristalsis ($\geq$2 times/3 min), whereas 29 patients (56%) exhibited a low frequency of peristalsis (0 or 1 time/3 min) during the implantation phase. Moreover, after the MRI examination, 10 of 29 patients (34%) with uterine myomas in the low-frequency group achieved pregnancy, whereas none of 22 patients (0%) in the high-frequency group achieved pregnancy, implying that abnormal peristalsis of patients with uterine myomas plays a role in infertility. After our first study, some of the patients with uterine myomas who did not achieve pregnancy underwent myomectomy. In this study, we examined the effect of myomectomy on uterine peristalsis and pregnancy rate in patients with high peristalsis.

Materials and Methods

The inclusion criteria for this study were as follows: (1) Patients who were infertile for at least 24 months with intramural uterine myomas. The patients who had severe symptoms related to myomas were recruited to this study if their infertility period was longer than 12 months; (2) Patients who had no other significant infertility factors in the screening test, such as anovulation, corpus luteum insufficiency, tubal disease, or abnormal semen analysis of the partner; (3) Patients who underwent myomectomy; (4) Patients who underwent MRI before and after myomectomy (referred to as first and second MRI, respectively) and during the time of implantation window (luteal phase day 5–9) and who exhibited abnormal uterine peristalsis with a frequency of uterine peristalsis that was $\geq$2 times/3 min before surgery.

In detail, the patients had regular menstrual cycles of about 28 days. Their basal levels of serum follicle-stimulating hormone, leutinizing hormone and prolactin on menstrual cycle days 3 to 5 were within normal range (criteria: follicle-stimulating hormone 3.5–12.5 mIU/mL, leutinizing hormone 2.4–12.6 mIU/mL, and prolactin 4.9–29.3 ng/mL). Their serum estradiol and progesterone concentrations in the midluteal phase were greater than 100 pg/mL and 10 ng/mL, respectively. The patients had no tubal obstruction detected on hysterosalpingography. Sperm concentration of the partner was at a level greater than 20×10^6/mL (World Health Organization, 1992). After screening tests were performed, ovarian functional status was monitored predominantly by basal body temperature (BBT) chart. Ovulation was determined by analysis of BBT graphs, wherein a rise in temperature of at least 0.2° C above the preceding 6 days that was completed in less than 48 hours and sustained for at least 11 days indicated that ovulation had occurred [6]. All patients included in this study showed unequivocal biphasic cycles in their BBT chart. We designated the day showing elevated temperature of at least 0.2° C as luteal phase day 1. MRI was performed before and after myomectomy during the time of implantation window (luteal phase days 5–9), judged retrospectively by BBT chart (evaluated by gynecologists O.Y., T.H.). The conditions for cine mode have been described elsewhere [5,7]. MRI studies were performed with a 1.5-T magnet unit (MRI machine from Siemens Medical Systems at Takinogawa Clinic or from GE Healthcare at Teikyo University) with a 6-ch array coil. Under quiet respiration, a total of 30 serial images were obtained by single-shot fast spin-echo sequence (echo time and repetition time [TR/TE] = 6000/78 msec, field of vision = 240 mm, slice thickness = 10 mm, matrix = 256 × 256), every 6 seconds/3 min in the midsagittal plane of the uterus. All images in 1 study were summated into 1 image and displayed sequentially on the cine mode display at 250-millisecond intervals. Subsequently, conventional axial and sagittal T_2-weighted images (TR/TE = 4000–4720/90–111 msec) and axial T_1-weighted images (TR/TE = 400–550/7.0–8.5 msec) were obtained to detect uterine myomas. One radiologist (T.H) interpreted the images without information about patients' menstrual cycles. Evaluation points included (1) perception of movement of the junctional zone on the cine mode display and (2) frequency of that movement, if perceivable. Patients were divided into 2 groups on the basis of the frequency of uterine peristalsis; less than 2 times/3 min (low-frequency group) and greater than or equal to 2 times/3 min (high-frequency group), as described [8].

Infertility treatments were performed as described [5]. Briefly, ovarian follicle growth was checked frequently, with transvaginal ultrasonography, in the absence of any drugs (natural cycle) or with clomiphene citrate or human menopausal gonadotropin for 2 to 3 courses, respectively. Clomiphene citrate (50–100 mg) was started on cycle day 5 for 5 days. Human menopausal gonadotropin was administered for 75 to 150 m IU on cycle day 3 and continued according to ovarian response. The size of the follicles was monitored until the diameter of the leading follicle reached 18 mm or greater, and the timing of ovulation was estimated. In some cases, human chorionic gonadotrophin at a dose of 5000 IU was administered. Intrauterine insemination was performed when motile sperm concentration was $<20 \times 10^6$/mL. Luteal phase support was not performed. After the first MRI, the patients received infertility treatment at Teikyo University for at least 4 months before undergoing myomectomy.

In this study, 15 patients fulfilled the criteria. Of the 15 patients undergoing myomectomy, 1 case was an abdominal myomectomy, 7 cases were laparoscopic myomectomies, and 7 cases were laparoscopically assisted myomectomies, a procedure that used a small abdominal incision to remove the myomas. The patients' characteristics are summarized in Table 1. The infertility period shown in Table 1 is the timing when the first MRI was obtained. One patient (case 3 in

Table 1

Characteristics of patients and the findings of first MRI

Case	Age	Infertility	Infertility period (mo.)	Number of myomas	Maximum diameter (mm)
1	41	Sec	48	6	120
2	37	Prim	51	2	75
3	29	Sec	4	1	73
4	38	Prim	24	6	50
5	38	Sec	21	3	45
6	38	Prim	24	5	55
7	37	Prim	24	10	50
8	41	Prim	60	1	80
9	37	Sec	24	5	55
10	38	Prim	52	2	85
11	36	Prim	24	2	45
12	37	Prim	24	1	30
13	37	Prim	24	10	70
14	36	Prim	72	1	50
15	40	Prim	84	1	60

Prim = primary; Sec= secondary.

Fifteen infertility patients, who had intramural myomas and exhibited abnormal uterine peristalsis (≥2 times/3 minutes) in their first MRI, underwent myomectomy and a second MRI. Clinical characteristics, including age, primary or secondary infertility, the period of infertility (month), the number of myomas and the maximum diameter (mm) of myoma at their first MRI test are shown.

Table 1) visited our hospital and underwent the first MRI test at 4 months of her infertility period. She had severe hypermenorrhea and was refractory to the infertility treatment for 8 months; therefore she underwent myomectomy at 12 months of her infertility period. After the second MRI, which was obtained after myomectomy, patients resumed infertility treatment and continued for at least 8 months with the treatment strategy described above, with the exception of one patient who chose in vitro fertilization (IVF) treatment.

Data regarding age, number of myomas and maximum diameter of myomas were expressed as median with minimum-maximum range. The difference in pregnancy rate was analyzed by 2 × 2 contingency table analysis.

Results

The Effect of Myomectomy on Uterine Peristalsis

Fifteen patients with infertility who had intramural myomas and exhibited abnormal uterine peristalsis underwent myomectomy and a second MRI test. In the second MRI test, we confirmed that that all uterine myomas observed before surgery had been removed.

The frequency of uterine peristalsis was evaluated before and after surgery (Table 2). In patients who exhibited high peristalsis before surgery (≥2 times/3 min, n = 15), the uterine peristalsis was normalized in 14 patients (0 or 1 time/3 min), whereas 1 patient (case 11) continued to exhibit high uterine peristalsis (5 times/3 min before surgery, and 3 times/3 min after surgery).

Pregnancy after Myomectomy

After myomectomy and the second MRI, patients resumed infertility treatment for at least 8 months, and the

Table 2

Frequency of uterine peristalsis before and after surgery (per 3 minutes), surgical procedure, and pregnancy

Case	Peristalsis frequency (before surgery)	Peristalsis frequency (after surgery)	Operation	Pregnancy	Time to pregnancy (mo.)	Time of treatment (mo.)
1	6	0	Abdominal	YES	3	
2	6	1	LAM	YES	5	
3	4	1	LM	YES	4	
4	4	1	LAM	YES	1	
5	3	0	LAM	YES	2	
6	3	0	LAM	YES	4	
7	3	1	LAM	No		16
8	4	0	LM	No		15
9	3	1	LAM	No		13
10	4	0	LM	No		12
11	5	3	LM	No		11
12	4	0	LM	No		11
13	5	0	LAM	No		9
14	4	0	LM	No		8
15	2	0	LM	No		9

Abdominal = abdominal myomectomy; LAM = laparoscopically assisted myomectomy; LM = laparoscopic myomectomy.

Fifteen patients with infertility, who had intramural myomas and exhibited abnormal uterine peristalsis (≥2 times/3 minutes) in their first MRI, underwent myomectomy and a second MRI. The frequency of uterine peristalsis per 3 minutes before and after surgery is shown. The surgical procedure of abdominal myomectomy, laparoscopically assisted myomectomy, or laparoscopic myomectomy was shown. After myomectomy, the range of fertility treatment period (month) for both those who conceived (Yes) and those who did not (No) was shown.

pregnancy rate was evaluated (Table 2). Six of 15 patients achieved pregnancy (n = 15, pregnancy rate: 40%). In detail, 5 conceptions were achieved in a natural cycle, in which patients underwent ultrasonography to check follicular growth and received instruction with regard to the timing of intercourse (cases 1-5), and 1 case (case 6) was achieved with IVF techniques, which was done at an infertility clinic elsewhere. This patient had not attempted IVF techniques before undergoing myomectomy and did not try non-IVF treatment after the surgery. All 6 pregnancies were intrauterine and reached term. The birth rate was 6 of 15 patients (40%).

Discussion

During the implantation phase, it is well known that uterine peristalsis is dramatically reduced, which is believed to facilitate implantation of the embryo to the endometrium [8–10]. Using a cine mode MRI display, we have confirmed that no uterine corporal peristalsis was noted in the healthy volunteers during the mid- and late-luteal phases [7]. Furthermore, in the previous study, we found that less than half of the patients with intramural myomas exhibited abnormal uterine peristalsis during the mid-luteal phase. Interestingly, in the high-frequency peristalsis group, no patients achieved pregnancy, whereas one third of patients in the low-frequency peristalsis group achieved pregnancy in the presence of myomas [5]. These data suggest that abnormal uterine peristalsis caused by intramural myomas could be one of the factors causing infertility. To further examine this hypothesis, we investigated whether myomectomy for patients in the high-frequency peristalsis group is a constructive method to normalize uterine peristalsis. Here, we examined the same patients assessed in the previous study.

As shown in Table 2, myomectomy reduced the frequency of abnormal peristalsis in all patients, and the peristalsis rate returned to normal range (0 or 1 time/3 minutes) in 14 of 15 patients. Moreover, 6 of 14 patients achieved pregnancy after myomectomy.

A correlation between uterine peristalsis rates and pregnancy has previously been demonstrated [9,10]. With ultrasonography, Fanchin et al [9] examined the uterine peristalsis of patients with infertility who do not have uterine abnormalities and found a negative correlation between the frequency of uterine peristalsis on the day of embryo transfer and pregnancy outcome. These results suggest that high-frequency endometrial waves on the day of embryo transfer may negatively influence transfer outcome, perhaps by expulsion of the embryos from the uterine cavity [9].

Likewise, our previous data suggest that abnormal uterine peristalsis has a negative impact on implantation. In that study of 22 patients who exhibited high-frequency peristalsis, none achieved pregnancy (pregnancy rate; 0 of 22 patients [0%]) [5]. In this study, we found that myomectomy returned peristalsis rates to normal in these patients, with a subsequent increase in pregnancy rates (6 of 15 patients [40%]). Although there is a possibility of type I error because of the small sample number, the pregnancy rate was improved significantly after surgery ($p < .0012$). Therefore these data might also suggest that abnormal uterine peristalsis has a negative impact on implantation.

In response to myomas, increased peristalsis may act as a mechanism to expel embryos from the uterus. Alternatively, estrogen is known to induce uterine peristalsis [11], and increased aromatase expression has been observed in uterine myomas [12]. Thus the elevated aromatase might result in elevated tissue estrogen concentration, which, in turn, could increase the rate of peristalsis. However, the precise mechanism by which myomas induce peristalsis remains unclear and requires further study.

In summary, we found that myomectomy reduced the frequency of uterine peristalsis in patients who had exhibited an abnormally high frequency of peristalsis before surgery. Moreover, we found that myomectomy increased the pregnancy rate in patients who had exhibited a high frequency of peristalsis. These findings suggest that the presence of uterine myomas might induce abnormal uterine peristalsis in some patients, leading to infertility, and that myomectomy may improve fertility in these patients.

Although the management of intramural type myomas continues to be difficult [1,2], cine mode MRI might have the potential to select patients who should undergo surgery. Because this study was preliminary, we made clinical decisions for the treatment of myomas not on the basis of the findings of cine mode MRI but on the traditional therapeutic strategy in which patients who were refractory to the infertility treatment had a choice to undergo myomectomy. Further randomized study with an increased number of subjects is warranted.

Acknowledgments

We thank Dr. Heather M. Martinez for her helpful discussion and critical reading of the manuscript. We thank Dr. Yasufumi Shimizu, Dr. Kouji Motoyama, and Dr. Yasuhiro Kawamura (Denentoshi Ladies' Clinic), Dr. Kenichi Tatsumi (Umegaoka Women's Clinic), Dr. Susumu Tokuoka (Tokuoka Women's Clinic), Dr. Ryo Matsuoka (Tokyo Hitachi Hospital), and Dr. Takayoshi Ogawa (Ogawa clinic), Dr. Masataka Furuya, and Dr. Yasunori Yoshimura (Keio University), Dr. Hiroko Tsuchiya, Dr. Yoko Tokura, and Dr. Miki Nakao (Teikyo University Mizonokuchi Hospital), Hisahiko Hiroi (Hiroi Women's Clinic), Fumikazu Kotsuji (Fukui University), Dr. Kaori Koga, and Dr. Yuji Taketani (Tokyo University) for their supporting our study. We also thank Mr. Ryuji Nojiri and Mr. Yoshitsugu Funatsu (Takinogawa Clinic) and Mr. Mitsuru Harako (Teikyo University Mizonokuchi Hospital) for their technical assistance.

References

1. Donnez J, Jadoul P. What are the implications of myomas on fertility? A need for a debate? *Hum Reprod.* 2002;17:1424–1430.

2. Somigliana E, Vercellini P, Daguati R, Pasin R, De Giorgi O, Crosignani PG. Fibroids and female reproduction: a critical analysis of the evidence. *Hum Reprod Update.* 2007;13:465–476.
3. Richards PA, Richards PD, Tiltman AJ. The ultrastructure of fibromyomatous myometrium and its relationship to infertility. *Hum Reprod Update.* 1998;4:520–525.
4. Fujiwara T, Togashi K, Yamaoka T, et al. Kinematics of the uterus: cine mode MR imaging. *Radiographics.* 2004;24:e19.
5. Yoshino O, Hayashi T, Osuga Y, et al. Decreased pregnancy rate is linked to abnormal uterine peristalsis caused by intramural fibroids. *Hum Reprod.* 2010;25:2475–2479.
6. Ayres-de-Campos D, Silva-Carvalho JL, Oliveira C, Martins-da-Silva I, Silva-Carvalho J, Pereira-Leite L. Inter-observer agreement in analysis of basal body temperature graphs from infertile women. *Hum Reprod.* 1995;10:2010–2016.
7. Orisaka M, Kurokawa T, Shukunami K, et al. A comparison of uterine peristalsis in women with normal uteri and uterine leiomyoma by cine magnetic resonance imaging. *Eur J Obstet Gynecol Reprod Biol.* 2007;135:111–115.
8. Togashi K. Uterine contractility evaluated on cine magnetic resonance imaging. *Ann N Y Acad Sci.* 2007;1101:62–71.
9. Fanchin R, Righini C, Olivennes F, Taylor S, de Ziegler D, Frydman R. Uterine contractions at the time of embryo transfer alter pregnancy rates after in-vitro fertilization. *Hum Reprod.* 1998;13:1968–1974.
10. Fanchin R, Ayoubi JM. Uterine dynamics: impact on the human reproduction process. *Reprod Biomed Online.* 2009;18(Suppl 2):57–62.
11. Mueller A, Siemer J, Schreiner S, et al. Role of estrogen and progesterone in the regulation of uterine peristalsis: results from perfused non-pregnant swine uteri. *Hum Reprod.* 2006;21:1863–1868.
12. Bulun SE, Imir G, Utsunomiya H, et al. Aromatase in endometriosis and uterine leiomyomata. *J Steroid Biochem Mol Biol.* 2005;95:57–62.

Toll-Like Receptor-3 Ligation-Induced Indoleamine 2, 3-Dioxygenase Expression in Human Trophoblasts

Bo Wang, Kaori Koga, Yutaka Osuga, Ingrid Cardenas, Gentaro Izumi, Masashi Takamura, Tetsuya Hirata, Osamu Yoshino, Yasushi Hirota, Miyuki Harada, Gil Mor, and Yuji Taketani

Department of Obstetrics and Gynecology (B.W., K.K., Y.O., G.I., M.T., T.H., O.Y., Y.H., M.H., Y.T.), University of Tokyo, Tokyo 113-8655, Japan; and Department of Obstetrics and Gynecology and Reproductive Science (I.C., G.M.), Yale University School of Medicine, New Haven, Connecticut 06520

Indoleamine 2,3-dioxygenase (IDO) is an enzyme that degrades an essential amino acid, tryptophan, and plays a role in inhibiting the proliferation of T cells and intracellular pathogens. Inhibiting IDO in mice leads to fetal rejection, suggesting its significance in establishing pregnancy. Toll-like receptor 3 (TLR-3) is a key component of the innate immune system that recognizes viral double-stranded RNA and triggers immune reactions by producing type I interferon. Using a human trophoblast cell culture system, we studied the effect of TLR-3 ligation on IDO expression and function by treating trophoblasts with polyinosinic-polycytidylic acid [poly(I:C)] (a synthetic double stranded RNA, which mimics viral RNA). Real-time PCR and Western blot analysis revealed that IDO mRNA and protein expression was significantly induced by poly(I:C). The activity of IDO was also increased by poly(I:C) given that the L-kynurenine concentrations were elevated in conditioned media. Conditioned media from poly(I:C)-treated trophoblasts were found to inhibit the proliferation of human T cells significantly. Poly(I:C) was also shown to induce interferon (IFN)-β mRNA expression in trophoblasts. Recombinant human IFN-β increased IDO mRNA expression in trophoblasts more rapidly than poly(I:C). Pretreating with neutralizing antibody against IFN-β significantly suppressed IDO induction by poly(I:C). Collectively we have demonstrated that ligation of TLR-3 by poly(I:C) induces IDO expression in human first-trimester trophoblasts via an IFN-β-dependent pathway. These findings suggest that upon viral infection, trophoblasts induce IDO and in turn contribute to antimicrobial activity and maintenance of fetomaternal tolerance. (*Endocrinology* 152: 4984–4992, 2011)

The fetomaternal interface is an immunologically unique site that must maintain host defense against possible pathogens and promote tolerance to the allogeneic fetus (1). Therefore, the immune system at the fetomaternal interface must be precisely controlled to meet the paradoxical task of defending against potential pathogens without compromising fetal survival. In this context, innate immune responses against microorganisms at the fetomaternal interface play a significant role (1, 2).

Cells of the innate immune system express a series of receptors known as pattern recognition receptors that recognize and bind to sequences known as pathogen-associated molecular patterns, which are uniquely expressed on the surface of microorganisms. Toll-like receptors (TLR) are the major family of pattern recognition receptors. To date, 10 functional human TLR have been characterized and each TLR responds to a particular ligand (3). For example, TLR-4 mediates responses toward Gram-negative bacterial lipopolysaccharide (4), whereas TLR-3 mediates immune responses toward viral double-stranded RNA (dsRNA) (5). Indeed, TLR signals must strike a delicate balance between clearing infection and causing pathological effects on the host.

ISSN Print 0013-7227 ISSN Online 1945-7170
Printed in U.S.A.

doi: 10.1210/en.2011-0278 Received March 10, 2011. Accepted August 30, 2011.
First Published Online September 27, 2011

Abbreviations: BrdU, 5-Bromo-2′-deoxyuridine; dsRNA, double-stranded RNA; FBS, fetal bovine serum; GAPDH, glyceraldehyde-3-phosphate dehydrogenase; IDO, indoleamine 2,3-dioxygenase; IFN, interferon; IRF3, IFN regulatory factor 3; poly(I:C), polyinosinic-polycytidylic acid; TLR, Toll-like receptor.

Among various types of cells in the fetomaternal interface, we focused on trophoblasts and investigated their roles in innate immunity. Studies have demonstrated that trophoblasts can recognize and respond to pathogens through the expression of TLR. For example, TLR-4 ligation promotes cytokine production, which may be involved in the pathogenesis of preeclampsia (6), whereas ligation of TLR-2 induces apoptosis in first-trimester trophoblasts (7). As a result of TLR-3 ligation, trophoblasts produce cytokines [including interferon (IFN)-β], chemokines that mount active immune responses (8) and antiviral molecules (9). All these findings show that trophoblasts respond to pathogens through TLR and further affect pregnancy.

Pregnant women may be exposed to a variety of pathogens including bacteria, fungus, and virus. Among them, viral infections cause highly diversified reactions to pregnant women, depending on the type of virus and the condition of hosts. Some are asymptomatic (10), but preterm labor (11–13) and fetal congenital anomalies of the central nervous system (14) and the cardiovascular system (15, 16) have been reported. Pregnancy can also increase susceptibility and the severity of viral infections such as H1N1 (17). This wide spectrum of the clinical consequence of viral infection during pregnancy implies various immunological reactions, especially in the placenta.

Indoleamine 2,3-dioxygenase (IDO) is the rate-limiting enzyme in the kynurenine pathway of tryptophan catabolism (18, 19). IDO plays a paradoxical role because it has antimicrobial activity in human cells (20) but also has immunosuppressive properties. Of note, IDO is crucial to the fetus in that it maintains maternal tolerance (21). IDO has been shown to be expressed (10) and functioning as an enzyme for tryptophan catabolism (22) in human trophoblasts. On the other hand, it has been recently reported that TLR ligation induces IDO expression in human cells such as gingival fibroblasts (23) and astrocytes (24). These findings prompted us to hypothesize that, in addition to previously reported molecules that are enhanced by TLR-3 ligation, IDO may also be induced by TLR-3 stimulation in trophoblasts, thereby contributing to viral resolution and the maintenance of maternal tolerance for fetus upon viral infection during pregnancy (10).

Materials and Methods

Reagents

Fetal bovine serum (FBS) was purchased from Life Technologies, Inc.-Invitrogen (Carlsbad, CA), and the same batch of serum was used in all experiments. Polyinosinic-polycytidylic acid [poly(I:C)], a synthetic analog of viral dsRNA, was purchased from Invivogen (San Diego, CA). Recombinant human IFN-β was purchased from PBL Biomedical Laboratories (Piscataway, NJ; 1 ng = 160 U). Rabbit antibody raised against human IFN-β was purchased from PBL for neutralization experiments. Protease inhibitor cocktail was purchased from Roche Diagnostics GmbH (Mannheim, Germany). Antihuman IDO mouse monoclonal antibody was purchased from Oriental Yeast (Nagahama, Japan). Normal mouse IgG1 was purchased from Amersham Biosciences (Little Chalfont, UK). Rabbit antihuman vinculin antibody (the loading control) was purchased from Santa Cruz Biotechnology, Inc. (Santa Cruz, CA). Horseradish peroxidase-conjugated antimouse antibody was purchased from Amersham Biosciences and antirabbit IgG from Santa Cruz Biotechnology. The enhanced chemiluminescence Western blotting system was purchased from Amersham Biosciences. All other reagents were purchased from Sigma-Aldrich Corp. (St. Louis, MO) unless stated otherwise.

Isolation and culture of trophoblasts from first-trimester placenta

First-trimester placentas (7–12 wk of gestation, n = 9) were obtained from elective termination of normal pregnancies performed after obtaining written informed consent under a study protocol approved by the Institutional Review Board of the University of Tokyo. Women's ages ranged from 18 to 34 yr.

Primary trophoblasts from first-trimester placentas were prepared as described previously (25). Briefly, tissue specimens were washed with cold PBS to remove excess blood. Placental villi were scraped from fetal membranes, transferred to trypsin-EDTA (Life Technologies, Inc.-Invitrogen) digestion buffer with deoxyribonuclease I (15 U/ml) and incubated at 37 C for 20 min with shaking. An equal volume of DMEM/F12 (Life Technologies, Inc.-Invitrogen) containing 10% FBS was added to inactivate trypsin and the tissue was filtered through nylon cell strainers with apertures of 100 μm. Trophoblasts in the filtrate were centrifuged at 200 g for 5 min. The resultant cell pellet was resuspended in 5 ml of DMEM/F12 containing 10% FBS and layered onto 3 ml of Ficoll-Paque PLUS (GE Healthcare, Uppsala, Sweden) in a 15-ml conical tube. The tube was centrifuged at 120 × *g* for 20 min. The cellular interface containing trophoblasts was collected and resuspended in red blood cells lysis buffer at room temperature for 5 min and then centrifuged at 200 × *g* for 5 min. After washing with PBS once, the trophoblasts were incubated with anti-CD45 antibodies coupled to magnetic beads (Dynal Biotech, Oslo, Norway) for 20 min at 4 C to exclude contaminating leukocytes. Cells bound to the beads were removed by a magnetic collector, and the suspension containing unbound cells was centrifuged at 200 × *g* for 5 min. The resulting isolated cells were resuspended in DMEM/F12 containing 10% FBS, penicillin (100 U/ml), streptomycin (100 μg/ml), and amphotericin B (0.25 μg/ml) and cultured at 37 C/5% CO_2. Purification of the trophoblasts was determined by immunocytochemical staining for CK7 (Sigma-Aldrich) and CD45 (Covance, Princeton, NJ). Purity of the trophoblasts was greater than 95% as determined by positive staining for CK7 and negative staining for CD45.

Culture of cell line

The immortalized trophoblast cell line, Swan 71, which was derived by telomerase-mediated transformation of 7-wk cytotro-

phoblasts (26), was cultured at 37 C/5% CO_2 in RPMI 1640 supplemented with 10% FBS and antibiotics.

Treatment of trophoblasts with poly(I:C), IFN-β, and antibodies

When the trophoblasts reached 70–80% confluence in 1–2 d, media were removed and replaced with fresh media containing 10% FBS. To evaluate the effect of poly (I:C) on mRNA and protein expression of IDO and IFN-β, primary trophoblasts were treated with poly(I:C) as indicated. In time-course experiments, Swan 71 cells were incubated with either poly(I:C) (10 μg/ml) or IFN-β (2.5 ng/ml) for the time period indicated (0, 2, 4, 6, 8, 12, and 24 h). To neutralize IFN-β activity, primary trophoblasts were preincubated with rabbit antihuman IFN-β (20 μg/ml) or nonimmune rabbit IgG for 30 min and then stimulated by poly(I:C).

Quantitative RT-PCR

Total RNA was isolated from cells using an RNAeasy minikit (QIAGEN, Hilden, Germany) and then treated with ribonuclease-free recombinant deoxyribonuclease (Roche Diagnostics GmbH). Reverse transcription was performed using ReverTra Ace (Toyobo, Osaka, Japan). One microgram of total RNA was reverse transcribed in a 20-μl total volume. PCR amplification was performed using the LightCycler 480 System (Roche Applied Science, Mannheim, Germany). IDO primers (sense, 5′-GGTCATGGAGATGTCCGTAA-3′; antisense, 5′-ACCAATAGAGAGACCAGGAAGAA-3′) were used to amplify a 227-bp fragment. IFN-β primers (sense, 5′-GCTCTCCTGTTGTGCTTCTCCACTACAGC-3′; antisense, 5′-CTGACTATGGTCCAGGCACAGTGACTGTACTCC-3′) were used to amplify a 476-bp fragment. Glyceraldehyde-3-phosphate dehydrogenase (GAPDH) primers (Toyobo) (sense, 5′-ACCACAGTCCATGCCATCAC-3′;antisense,5′-TCCACCACCCTGTTGCTGTA-3′) were used to amplify a 452-bp fragment. The conditions for PCR were as follows: IDO, 45 cycles at 95 C for 10 sec, 62 C for 10 sec, and 72 C for 10 sec; IFN-β, 45 cycles at 95 C for 10 sec, 72 C for 10 sec, and 72 C for 20 sec; GAPDH, 30 cycles at 95 C for 10 sec, 64 C for 10 sec, and 72 C for 18 sec. All PCR were followed up with melting curve analysis. The expression level of each mRNA was normalized according to GAPDH levels in each case.

Western blot analysis

Cultured trophoblasts were homogenized in a lysis buffer [10 mM Tris-HCl, 50 mM NaCl, 2 mM EDTA, 1% Triton X-100 (pH 7.0)] with a protease inhibitor cocktail. Protein (30 μg) was separated by 10% SDS-PAGE and then transferred onto nitrocellulose membranes. The blots were blocked in Tris-buffered saline-0.1% Tween 20 containing 5% nonfat milk and then incubated with antibodies at 4 C overnight. The membranes were incubated with primary antibodies; antihuman IDO antibody (1:800) or antihuman vinculin antibody (1:400) as a loading control. The membranes were further incubated with a secondary antibody, a horseradish peroxidase-conjugated antimouse (1:1000) or antirabbit (1:5000) IgG for 1 h at room temperature. Signals were developed using an enhanced chemiluminescence Western blotting system. Densitometric analysis was performed using ImageJ (National Institutes of Health, Bethesda, MD).

Kynurenine assay

IDO-dependent catabolism of tryptophan produces kynurenine. Hence, the enzymatic activity of IDO can be evaluated by measuring the level of kynurenine in conditioned media (27). After stimulating Swan 71 cells with poly(I:C), 70 μl of Swan 71 conditioned media was mixed with 35 μl of 30% trichloroacetic acid, vortexed, and centrifuged at 8000 × *g* for 5 min. Then 75 μl of the supernatant was added to an equal volume of Ehrlich reagent (100 mg of *p*-dimethylbenzaldehyde in 5 ml of glacial acetic acid) in a 96-well plate, and the absorbance was read at an OD of 492 nm. The concentration of kynurenine was determined by referring to a standard curve of defined kynurenine concentrations (0–100 μM).

Analysis of T cell proliferation

To evaluate the effect of IDO produced by trophoblasts on T cell proliferation, we cultured T cells with conditioned media from the trophoblast culture and analyzed DNA synthesis in T cells by measuring 5-bromo-2′-deoxyuridine (BrdU) incorporation. Conditioned media were prepared by culturing Swan 71 cells with or without poly(I:C) for 24 h. T cells were isolated from peripheral blood mononuclear cells from healthy, nonpregnant volunteers by using a CD4-positive T cell isolation kit II (Miltenyi Biotec, Bergisch Gladbach, Germany) and stimulated with phytohemagglutinin (5 μg/ml). The cells (2×10^5 cells in 100 μl media per well) were cultured in 96-well flat-bottom plates, containing 90% (vol/vol) Swan 71 cells' conditioned media. To confirm the tryptophan-catabolizing effect of IDO, L-trypotophan (100 μM) was added to the conditioned media. After 72 h, 10 μl of BrdU solution was added to each well and incubated for an additional 24 h. BrdU uptake was measured using the cell proliferation ELISA system based on BrdU incorporation (Amersham Biosciences). The immune complexes were detected by the subsequent substrate reaction, and the resultant color was read at 450 nm in the DigiScan microplate reader (ASYS Hitech GmbH, Eugendorf, Austria).

Statistical analysis

Data analysis was performed using the statistical software package SPSS for Windows (Chicago, IL). All data were checked for their normal distribution by using the Kolmogorov-Smirnov test, and if significant, nonparametric statistical analysis was applied. Parametric variables underwent the Student's *t* test. Statistical significance was considered as $P < 0.05$.

Results

Poly(I:C) induced IDO mRNA and protein expression in the first-trimester trophoblasts

RT-PCR results revealed that first-trimester trophoblasts did not express IDO mRNA constitutively. In contrast, IDO mRNA expression was induced by 12 h treatment of poly(I:C) (10 μg/ml) (Fig. 1A). IFN-γ, which is known to induce IDO in many cell types, was used as a positive control (28, 29). The induction was dose dependent (Fig. 1B). We further analyzed protein expression of IDO by Western blot analysis. Similar to mRNA results,